The Essential Work of Fracture Method for the Characterisation of Fusion Bonding in 3D Printed Short Carbon-Fibre Reinforced Polyamide 6 Thin Films

Qinghao He [a, b], Lin Ye [a,*] and Anthony J. Kinloch [c]

[a] Centre for Advanced Materials Technology, School of Aerospace, Mechanical and Mechatronic Engineering, University of Sydney, NSW 2006, Australia

[b] Research Institute of Advanced Composite Forming Technology and Equipment, Jiangsu Industrial Technology Research Institute (JITRI), Wuxi, China

[c] Department of Mechanical Engineering, Imperial College London, South Kensington Campus, London, SW7 2AZ, UK

*E-mail address: lin.ye@sydney.edu.au

Abstract

The fusion bonding between individual filaments of 3D printed short carbon-fibre reinforced polyamide 6 (SCF/PA6) in thin films manufactured using the fused filament fabrication (FFF) process has been studied. The thin films were deposited by an 'in-plane' mode or an 'interlayer' mode. The main characterisation technique employed was the essential work of fracture (EWF) method. Undertaking EWF tests on such thin films is shown to be a feasible and efficient way to evaluate the extent and quality of fusion bonding between individual filaments of the 3D printed SCF/PA6 composites. For example, firstly, for the 3D printed SCF/PA6 thin films it was readily evident that the extent of fusion bonding, i.e. the adhesion via molecular inter-diffusion, often termed the autohesion, between the filaments is the weakest, and the most variable, in the 3D printed SCF/PA6 thin films deposited via the interlayer mode. This was indicated by the lowest measured values of both the specific essential work of fracture, w_e, and the coefficient of determination, R^2, of 19.6 ± 3.9 kJ/m^2 and 0.05, respectively, for the interlayer printed SCF/PA6 thin films. Secondly, the quality of the 3D printed SCF/PA6 thin films deposited via the in-plane mode was significantly enhanced by the use of further compression moulding (CM) processing, since the value of R^2 increased from 0.77 to 0.92. The results clearly suggest the need to improve the extent and quality of fusion bonding between individual filaments printed using the FFF process when 3D printed components are made for practical applications.

Keywords: Fusion bonding; Fused filament fabrication; Essential work of fracture; Short carbon-fibre reinforced polyamide 6; Process–structure–property relationships.

1. Introduction

The fused filament fabrication (FFF) process is the most extensively used 3D printing method among many different kinds of additive manufacturing technologies and is well-known for its cost-effectiveness, easy access, fabrication flexibility, etc. [1]. In the FFF process, the component is fabricated by the deposition of molten polymeric filaments which are fused together. Therefore, the mechanical performance of the manufactured component is very dependent upon the extent and quality of the fusion bonding between the deposited filaments. Now, for good and consistent fusion bonding between the deposited filaments, a first key requirement is the attainment of intimate molecular contact between two filaments, so that the second key requirement of good intrinsic adhesion via molecular inter-diffusion (i.e. autohesion) between the two filaments can then occur.

Currently, with the rapid developments in this field, the options of available thermoplastics for use as the filament feedstock have increased steadily, ranging from pure polymers such as polyamides, poly(ether-ether-ketone), etc. to fibre-reinforced polymer composites [2-5]. However, for a given feedstock material, components manufactured using the FFF process generally suffer from a significantly reduced mechanical performance compared to those made using conventional manufacturing methods, such as injection or compression moulding. This observation is mainly attributed to the aspect mentioned above, namely inadequate fusion bonding between the filaments being developed during the FFF process.

Considerable efforts have been made during the last two decades to address the problems of the relatively poor mechanical performance of 3D printed components manufactured by the FFF process and, thereby, enhance their load-bearing capacity for structural applications. Many studies have focused on the optimisation of the printing parameters in order to improve the mechanical properties of the fabricated components, including the film layer thickness, printing orientation, temperature of extrusion, etc. [6-8]. Additionally, the development of novel feedstock materials for the FFF process by adding reinforcements to the polymer has attracted intense interest, including the development of nanofibre reinforced composites [9], short-fibre reinforced composites [10-12], and continuous-fibre reinforced composites [5, 13, 14]. For example, Tekinalp et al. [15] have investigated the effects of adding short carbon-fibres (SCFs) to an acrylonitrile-butadiene-styrene (ABS) polymer by testing uniaxial tensile specimens manufactured using the FFF process. Compared to traditional compression moulded specimens, the 3D printed specimens possessed an increased tensile modulus and strength of 115% and 700%, respectively. They ascribed these increases to an improved orientation and dispersion of the SCFs in the specimens manufactured using the FFF process. They also stated that minimising the void formation during the 3D printing process, by improving the extent and quality of the fusion bonding between filaments, was a necessary development in order for the FFF process to reach its full potential.

The above work highlights the need for a quantitative characterisation of the fusion bonding between adjacent filaments which results from the FFF process. Several workers have attempted to use a fracture mechanics approach to achieve this goal. A test method to characterise the Mode-I (tensile opening) fracture toughness of specimens printed by the FFF process based on a modified double-cantilever beam (DCB) test has been proposed by Young et al. [16]. For example, the values of the fracture toughness of a 3D printed ABS polymer and a SCF-reinforced ABS (SCF/ABS) composite were found to be relatively low when compared with similar specimens that had been subjected to further compression moulding (CM). This was attributed to relatively fast cooling of the deposited materials, the presence of voids and, in the case of the SCF/ABS composite, poorly wetted fibres. Besides the DCB test to characterise the extent and quality of the fusion bonding, compact-tension tests have been conducted by Papon and Haque [17] using FFF printed polylactic acid (PLA) and SCF/PLA composites, where the functional relationships between the fibre content and the fracture properties for the SCF/PLA composites were explored. However, neither the modified double-cantilever beam nor the compact-tension test directly evaluate the extent and quality of fusion bonding between individual filaments of the 3D printed polymer, or composite, films. Therefore, He et al. [18] successfully developed a novel test method based upon the concepts of the essential work of fracture (EWF) approach to characterise the quality and extent of the fusion bonding between individual filaments of 3D printed polyamide (PA6) thin films, manufactured by the FFF process. They reported that the use of EWF tests was a feasible and efficient way to evaluate the fusion bonding, and that such tests could provide a valuable insight into the 3D printing quality of the FFF process. It should be noted, that the evaluation of the extent and quality of fusion bonding can also be indirectly undertaken in a semi-quantitative manner by using a mesostructural analysis with, for example, the variation of the neck growth between adjacent filaments being measured using optical microscopy [19, 20].

The present work aims to characterise the fusion bonding of adjacent filaments in thin films of 3D printed SCF-reinforced polyamide 6 (SCF/PA6) composites, manufactured using the FFF process, by employing the EWF method. Further, to identify the process–structure–property relationships, the mesostructures of the thin films are examined using optical microscopy. Thin films manufactured via both the 'in-plane' and 'interlayer' deposition modes are studied. The work firstly aims to define differences in the extent and quality of the fusion bonding, i.e. the adhesion via molecular inter-diffusion, between the filaments and also the mesostructures of the thin films developed during the deposition of the SCF/PA6 filaments, using the two different deposition modes. Secondly, the results obtained are compared to those from thin films of in-plane printed SCF/PA6 composites which have been further processed using CM, so as to try to enhance the extent and quality of the fusion bonding between the filaments. Thirdly, the results obtained are also compared to those from corresponding thin films of 3D printed non-reinforced (i.e. 'pure') PA6 polymers which have also been manufactured using the FFF process.

2. Experimental details and materials

2.1 Principles of the EWF test method

The EWF methodology has gained widespread acceptance for the fracture characterisation of thin films of ductile polymers and ductile short fibre-reinforced polymeric composites due to the relative ease and simplicity of this test method [18, 21-24], which uses the double edged-notched tension (DENT) test specimen. The EWF method has been shown to be applicable to thin films of ductile polymers and composites providing the following criteria are met: (a) full ligament yielding occurs prior to crack initiation, (b) self-similar load-displacement curves are measured, (c) plane-stress conditions prevail and (d) the volume of the outer plastic dissipation zone approximately scales with the square of the ligament. More details about these required test conditions can be found in a comprehensive review [21] and these four criteria are all met for the present EWF tests, as shown previously [18] and as discussed below. Thus, in accordance with the theory of the EWF method, the total energy dissipated during an EWF test is:

$$W_f = \int_0^{\delta_C} P \, d\delta \quad (1)$$

where W_f is the total work of fracture, P is the tensile load applied to the specimen and δ is the corresponding measured displacement until complete failure occurs. In principle, the term W_f can be divided into two parts: the essential work done in tearing the ligament, W_e, and the plastic work done in a more diffuse zone, W_p, surrounding the crack tips. For plane-stress conditions, W_e is proportional to the length of the ligament, L, while W_p is proportional to L^2, and thus Equation 1 can be re-written as:

$$W_f = W_e + W_p = w_e LT + \beta w_p L^2 T \quad (2)$$

where w_e is the specific essential work of fracture, w_p is the specific non-essential work, T is the thickness of the DENT specimen, and β is a shape factor. Hence, if both sides of Equation 2 are divided by the area of the ligament region (i.e. $L \times T$), the relationship between the specific total work of fracture, w_f, and the ligament length, L, will be:

$$w_f = w_e + \beta w_p L \quad (3)$$

Thus, if several DENT specimens with different ligament lengths are tested, then the value of w_f can be plotted against L, where the positive intercept of the least-squares regression-line would be w_e, with the slope being βw_p. The value of w_e so obtained was used to quantify the toughness of all the polymeric composite films manufactured in the present study and, more importantly, to evaluate the extent of fusion bonding developed during the FFF process [18].

Finally, in the linear-regression analysis, the coefficient of determination, R^2, can be deduced, which describes how the variation of the specific work of fracture, w_f, is directly related to the change in the ligament length, L:

$$R^2 = \left[\frac{1}{n-1}\sum_{i=1}^{n}\left(\frac{L_i - \bar{L}}{S_L}\right)\left(\frac{w_{f_i} - \overline{w_f}}{S_{w_f}}\right)\right]^2 \quad (4)$$

where n is the total number of EWF tests, w_{f_i} and L_i represent the specific work of fracture and the ligament length, respectively, from the i-th test and $\overline{w_f}$ and $\bar{L}$ are their mean values, respectively, and S_{w_f} and S_L are their standard deviations, respectively. Ideally, for a large number of EWF tests on a material of perfect consistency, i.e. without any experimental error, the value of R^2 is 1.0. Now, for the EWF tests, a relatively low value of R^2 suggests an inconsistent quality of the tested material. Therefore, besides using the term w_e to evaluate the extent of fusion bonding developed during the FFF process, the coefficient of determination, R^2, gained from the linear regression analysis can be used as an indicator to assess the consistency of the printing quality of the 3D printed composite thin films [18].

2.2 Materials and specimen preparation

All the 3D printed films were manufactured via the FFF process using a desktop 3D printer (Markforged® Mark Two, USA) with a feedstock of filaments of 15 wt% of SCFs in a PA6 matrix (Onyx®, USA) [25]. A main advantage of using the SCFs/PA6 composite as the feedstock for the filaments is that the presence of the SCFs markedly increases the modulus of the filaments, compared to using the non-reinforced (i.e. pure) PA6 polymer. Hence, the presence of the SCFs in the filaments increases the overall stiffness of the component manufactured using the FFF process. The default pre-set printing parameters were used with the temperature set at 275^{o}C and a deposition speed of 16 mm/s. The diameter of the extruded filaments of SCF/PA6 was 0.4 mm before deposition.

DENT specimens were prepared from the thin films of the 3D printed SCF/PA6 composites, deposited in the 'in-plane' and 'interlayer' modes, respectively, using the FFF process, see Figure 1. Now, Figure 1 (a) shows a schematic of the single-layer thin film (100×85×0.125 mm) which was used to characterise the in-plane fusion bonding between individual filaments, whereas a single-filament box (110×110×90 mm) with the nominal thickness of 0.4 mm of each side wall was used to evaluate the interlayer (i.e. through-thickness) fusion bonding, as shown in Figure 1 (b). To study if more extensive molecular inter-diffusion of the filaments could be obtained, SCF/PA6 thin films were firstly printed using the FFF process, being deposited by the in-plane mode but now using two deposited layers with a nominal thickness of 0.25 mm. They were then subsequently hot-pressed using a compression moulding (CM) press. This moulding operation was undertaken at 220^{o}C and a pressure of 2 MPa was applied for 5 minutes to the SCF/PA6 composite thin film, followed by allowing natural cooling to room temperature.

Figure 2(a) shows a schematic diagram of a DENT specimen. The nominal dimensions (W×H×T) of the DENT specimens were 30×80×0.125 mm^3 (cut from the single-layer film printed via the in-plane deposition mode) or 30×80×0.4 mm^3 (cut from the single-filament box printed via the interlayer deposition mode). As indicated by the two rectangles in Figure 1(a), two DENT specimens could be cut, in the *x*-*y* plane, from the single-layer of in-plane printed composite thin film. Further, as indicated by the two rectangles in Figure 1(b), two DENT specimens could be cut, in the *z*-*x* plane, from each side of the single-filament box of interlayer printed composite. For the cutting, a laser cutter (Fusion M2, Epilog, USA) was used. By locating the DENT specimens within the 3D printed films as centrally as possible any edge effects resulting from the printing process were minimised. For each DENT specimen, both sides were notched by using a new, sharp razor blade, in order to obtain a ligament with a nominal length ranging from 2 mm to 10 mm. DENT specimens with equally spaced values of the ligament length were prepared. The upper-bound of the ligament length was taken to be one-third of the specimen width to avoid edge effects, whilst the lower-bound value was selected as being greater than five times of the thickness of the film in order to meet the necessary plane-stress conditions [24]. It should be noted that for the two DENT specimens that were cut from the same printed film, the ligament length was varied so as to avoid any 'batch effect'.

2.3 Experimental methods

To measure the length of the short carbon-fibres in the Onyx® filament, a small segment of the SCF/PA6 composite filament was placed in a beaker filled with formic acid (F0507, Sigma-Aldrich, Australia). After the PA6 matrix had completely dissolved, the mixture was filtered through filter paper. The retained short fibres were dried and measured using an optical microscope.

The thermal properties of the 3D printed SCF/PA6 composite films, with and without CM being employed after the FFF process, were evaluated using differential scanning calorimetry (DSC), namely a 2920 Modulated DSC (TA Instruments, USA). The specimens were ~10 mg in mass and were encapsulated in an aluminium pan and heated at a rate of 10°C/min from 30 to 300°C in a nitrogen atmosphere, with the heat flow recorded during the test.

The ligament length of each DENT specimen was measured using an optical microscope before performing the EWF test. As an example, an optical micrograph showing part of a 3D printed SCF/PA6 specimen, deposited via the in-plane mode, with a nominal ligament length of 2 mm, is given in Figure 2 (b). Clearly, from such optical micrographs the actual crack length can be measured accurately. The thickness of each DENT specimen was repeatedly measured three times with the aid of a precision micrometer, and the average thickness determined.

EWF tests were carried out using a universal testing machine (Instron 5567, USA) equipped with a 100 N load cell at a rate of test of 2 mm/min. The tests were performed in a controlled environment, i.e. at 25^{o}C and 60% RH. Sandpaper was placed inside the pneumatic grips to ensure firm clamping of the DENT specimen and a pre-load of ~ 0.2 N was applied to obtain alignment of the specimen (Figure 2 (c)). More than twenty specimens were tested for each type of EWF test, in order to get an accurate determination of w_e. All the EWF tests were video-recorded using a high-resolution camera that operated from the start of each EWF test. Thus, the fracture behaviour, e.g. the blunting of the cracks, the type of crack propagation, etc., could be readily studied and measured.

Several polished cross-sections of the 3D printed SCF/PA6 thin films that were cut from the in-plane and interlayer deposition mode specimens were observed using an optical microscope, see Figure 1, with the thickness of the thin films being measured by using image-processing software (ImageJ, NIH, USA). Additionally, to quantify the fibre-orientation distribution in the 3D printed composite films, without and with further compression moulding (CM), the films were examined using a transmission optical microscope, with more than one thousand fibres being assessed via the image-processing software.

3. Results: material properties and mesostructures

An optical micrograph of the SCFs from the SCF/PA6 composite feedstock filament, after removing the PA6 matrix, is presented in Figure 3, where a noticeable variation in the length of the fibres can be clearly observed. Based on measurements, using more than five optical micrographs, the lengths of the short fibres (of 7 μm in diameter) revealed a wide range from 35 μm to 245 μm, with an average of 105 μm. Significantly, these values are less than the nozzle diameter, i.e. 400 μm, of the equipment used for the FFF process.

Figure 4 shows typical DSC curves of 3D printed SCF/PA6 thin films deposited via the in-plane and interlayer modes, and the 3D printed film deposited via the in-plane mode with further CM processing. The crystallinity was calculated by taking the heat of fusion of the fully crystalline PA6 to be 230 J/g [26] and allowing for the 15 wt% of fibres present in the SCF/PA6. No clear differences in the melting temperatures, of ~200^{o}C, of the 3D printed SCF/PA6 thin films before and after CM are observed. However, there is a slight difference in the degree of crystallinity between the SCF/PA6 films printed via deposition using the in-plane or the interlayer modes, and also the thin film with further CM, with values of 19.5%, 21.1% and 17.4%, being measured, respectively. These relatively small variations are likely to arise from slight differences in the weight fraction of fibres in the 3D printed films.

Figure 5 shows optical micrographs of typical cross-sections of the three types of the SCF/PA6 thin films, i.e. (a) the in-plane printed SCF/PA6, (b) the interlayer printed SCF/PA6 and (c) the in-plane printed SCF/PA6 with further CM processing. Variations in the thickness of the thin films, along the height, *H*, of the DENT specimens, are clearly visible in the 3D printed SCF/PA6 films for both the in-plane and interlayer deposition modes, which both show a regular ridge–valley pattern. Specifically, the thickness ranges from 111 to 142 µm, with an average of 125 ± 11 µm, for the in-plane deposition mode and between 346 to 460 µm, with an average of 408 ± 49 µm, for the interlayer deposition mode, see Figure 5 (a) and (b). Furthermore, as may be seen from these figures, for both types of deposition mode, most of the SCFs appear as small bright dots across the section, indicating that they are predominantly orientated parallel to the printing direction due to the significant shear flow that occurs in the FFF process. In comparison, the in-plane printed SCF/PA6 film with further CM processing is obviously flattened by the further CM due to the pressure applied during this process. This may readily be seen from Figure 5 (c), where this film shows a relatively smooth surface along its height, *H*, in the DENT specimen, with no ridge–valley pattern and a uniform thickness with an average thickness value of 178 ± 7 µm.

To quantify the fibre-orientation distribution within the SCF/PA6 thin films, further mesostructural analyses were conducted to characterise the alignment of the SCFs, as shown in Figure 6. The angle of the fibre, relative to the longitudinal direction of the filament, was measured for about one thousand fibres to obtain the fibre-orientation distribution of the SCFs [27]. Multiple optical micrographs were taken using transmitted light, or reflected light, from polished sections of the films. In the (a) in-plane printed SCF/PA6 films and (b) interlayer printed SCF/PA6 films it is evident that almost all the SCFs preferentially align parallel to the printing direction, i.e. along the longitudinal direction of the filament, see Figures 6(a) and 6(b). The distribution of the fibre-orientation distribution can be fitted using a Gaussian function, with more than 65% of the SCFs distributed in the range of ±10° of the printing direction for both of these films. Indeed, for the in-plane printed SCF/PA6 films, in the *x*-*y* plane, there were 83% of fibres oriented in the range of ±20° relative to the printing direction, whilst for the interlayer printed SCF/PA6 film, in the *z*-*x* plane, there were 99.8% of fibres oriented in the range of ± 20° relative to the printing direction. By contrast, the SCFs were found to be distributed relatively randomly in the in-plane printed SCF/PA6 films with further CM processing, see Figure 6(c). This trend to a more random orientation, after further CM processing, is likely to arise from (a) the relatively short length of the SCFs and (b) the lack of any constraint on the films during the CM process.

4. Results: the EWF tests

4.1 In-plane deposition mode

Typical load versus displacement curves for the in-plane printed SCF/PA6 films with different ligament lengths from the EWF tests are shown in Figure 7 (a). As is evident, all the load versus displacement curves are very similar in shape, satisfying the critical prerequisite [18, 21, 24] for the EWF test methodology to be valid, i.e. criterion (b) as discussed in Section 2.1. It may also be observed that the area under the curves, after the maximum load has been attained, is much greater than that before the maximum load occurs, which indicates that slow crack propagation, crack tip blunting and considerable ductile deformation has occurred in the EWF test. Again, these observations confirm the validity of the EWF methodology with respect to testing the current 3D printed ductile thin films [18, 21, 24], and see Section 2.1. Figure 7 (b) shows photographs of the fracture behaviour of an in-plane printed SCF/PA6 film with a nominal 10 mm ligament length. With an increase in the applied tensile load, both of the sharp notch-tips begin to blunt slightly, followed by the initiation of stable crack propagation after the ligament fully yields. Upon the stable crack growth occurring, the load drops gradually as there is a decrease in the remaining ligament length, with a final sharp fall corresponding to the complete failure of the ligament. It should also be noted that gross, ductile yielding and necking of the ligament were observed in all the DENT specimens, which again confirms [18, 21, 24, 28, 29] the validity of the EWF method to characterise the fusion bonding developed in the 3D printed SCF/PA6 composite thin films.

As discussed in Section 2.1, a quantitative indicator of the quality of fusion bonding between the filaments, i.e. the specific essential work of fracture, w_e, can be extrapolated from a plot of w_f against L. The plot of all the experimental data, together with the linear-regression line, and the 95% confidence and prediction lines, are shown in Figure 7 (c). The value of w_e, i.e. the positive intercept of the fitted regression line, was determined to be 29.2 kJ/m^2, while the coefficient of determination, R^2, was 0.77.

4.2 Interlayer deposition mode

EWF tests were conducted using the interlayer printed SCF/PA6 thin films. As shown in Figure 8 (a), again, all the load versus displacement curves are very similar in shape, satisfying this critical prerequisite of the EWF test [18, 21, 24]. Furthermore, all the other criteria described above in Section 2.1 for the validity of the EWF approach are also met. However, as may be clearly seen, the interlayer printed SCF/PA6 films, with the same nominal ligament length, demonstrate a value of the peak load of more than double that measured for the in-plane printed films. This arises mainly from the greater thickness of the interlayer printed SCF/PA6 films, i.e. 0.4 mm versus 0.125 mm for the in-plane printed films. Comparing the stable crack propagation observed during the EWF tests for the interlayer printed films, to that observed in the in-plane films, it takes a much shorter time for the cracks from both tips to propagate through the whole ligament in the DENT specimens for the interlayer films. This occurs just after the maximum load is reached as is evidenced by a rapid drop of the load at this point, see Figure 8(b). Furthermore, as may be seen by comparing Figures 8 (b) and 7(b), a much smaller plastic zone is observed for the interlayer DENT specimens, which is reflected in the lack of noticeable thinning of the interlayer films during EWF testing. Finally, it should be noted that unstable crack growth was observed in some interlayer DENT specimens, especially when the ligament length was relatively large.

A plot of the total specific work of fracture, w_f, against the ligament length, L, was obtained for the interlayer printed SCF/PA6 films, see Figure 8 (c). A relatively large scatter in the experimental data is observed, as reflected by the wider confidence bands shown in Figure 8 (c), compared to Figure 7(c). The value of w_e was determined to be 19.6 kJ/m^2 accompanied by a very low value of R^2 of 0.05, which clearly reveals the poor consistency of the fusion bonding achieved by the FFF printing using the interlayer deposition mode. Moreover, the significant decrease of 33% in the value of w_e, compared to that for the composite film printed using the in-plane deposition mode, clearly reveals that the fusion bonding between filaments when an interlayer deposition mode is used is much weaker than that developed in the 3D printed SCF/PA6 films using the in-plane deposition mode.

4.3 In-plane deposition mode with further CM

Figure 9 (a) shows the typical load versus displacement curves of the in-plane printed SCF/PA6 thin films with further CM processing. From Figures 9(a) and 9(b), again all the criteria are met for the EWF methodology to be considered a valid approach to analyse the failure of these DENT test specimens, as discussed in Section 4.1. Compared to the results of the 3D in-plane (single-layer) printed SCF/PA6 film but with no further CM, see Figure 7 (a), there is now a significant increase in the maximum load for the same nominal ligament length. This mainly arises, of course, from the greater thickness of the 3D in-plane (double-layer) printed SCF/PA6 film with further CM processing, namely 178 ± 7 μm compared to 125 ± 11 μm.

Figure 9 (c) shows the experimental data of w_f versus L for the in-plane printed SCF/PA6 films with further CM processing, where the excellent linearity with very narrow confidence bands can be observed. The value of w_e was determined to be 25.2 kJ/m^2, with a high coefficient of determination, R^2, of 0.92.

5. The extent and quality of the fusion bonding between filaments

The values of both w_e and R^2 for all the 3D printed SCF/PA6 composite thin films are summarised in Table 1. And they are also compared to values for the non-reinforced (i.e. 'pure') PA6 thin films taken from [18], where the 'pure' PA6 films were fabricated using the same printing configurations. Several interesting observations may be made in terms of using these values to identify the extent and quality of fusion bonding in the 3D printed SCF/PA6 composite thin films.

Firstly, for the 3D printed SCF/PA6 composite thin films it is readily evident that the extent of fusion bonding, i.e. the adhesion via molecular inter-diffusion, often termed the autohesion [30, 31], between the filaments is the weakest, and the most variable, in the composite thin films deposited via the interlayer mode, as indicated by the lowest measured values of both w_e and R^2, respectively. The low value of R^2 arises due to significant defects in the mesostructures being formed during the FFF process when using the interlayer deposition mode. The reasons for this poor quality of the fusion bonding between the filaments are illustrated in Figure 10. For example, Figure 10 (b) reveals that there are many defects, e.g. flattened voids, in the fusion line between adjacent filaments where incomplete fusion has occurred. Now, such voids may especially develop and grow ahead of the main crack tips, where relatively high stress concentrations exist, and are shown in Figure 10 (c), where this EWF test was stopped during the rapid crack propagation stage so that the ligament was preserved without complete separation. The voids that develop at the crack tips, coupled with the relatively weak autohesion between the filaments, leads to the unstable crack growth that was seen in some of the EWT tests using the interlayer printed SCF/PA6 film. Indeed, such unstable crack growth is only observed in this type of interlayer printed SCF/PA6 composite film and occurs when the ligament suddenly ruptures at the very onset of the main cracks propagating. This is reflected in the very sharp drop in the load, see the load versus displacement curve shown in Figure 10 (a). Now, for good fusion bonding between the deposited filaments, a first key requirement is the attainment of intimate molecular contact between two filaments, so that the second key requirement of good intrinsic adhesion via molecular inter-diffusion (i.e. autohesion) between the two filaments can then occur. This first key requirement, of the attainment of intimate molecular contact, is largely governed by the external thermal energy and pressure [18, 19] available for this requirement. Now, a lack of sufficient thermal energy in the FFF process will cause a relatively large temperature gradient and a reduced fluidity, i.e. a higher viscosity, of the feedstock material forming the filament, especially given the presence of SCFs in the PA6 composite filament. Further, insufficient pressure from the depositing nozzle will also inhibit the formation of good fusion bonding. All of these factors will thus tend to lead to relatively weak fusion bonding between adjacent filaments in the interlayer printed SCF/PA6 composite films. Now, following the work reported in [18], the individual filaments in a 3D printed SCF/PA6 film will indeed cool down far more rapidly in a film deposited via the interlayer mode, as compared to those in an in-plane printed SCF/PA6 film. Furthermore, the nozzle pressure will be relatively low for the films printed via the interlayer deposition mode, since there is no lateral constraint offered by adjacent filaments, compared to the in-plane deposition mode. These processing effects therefore give rise to the relatively poor extent and quality of the fusion bonding between the filaments in the interlayer printed SCF/PA6 composite thin films, as evidenced by the associated low values in w_e and R^2. Finally, it is interesting to note that very similar observations were recorded [18] for the interlayer printed (non-reinforced) PA6 polymer thin films.

Secondly, for the 3D printed SCF/PA6 thin films deposited via the in-plane mode, the use of a further compression moulding (CM) process appears to have no significant effect on the extent of fusion bonding, since there is no significant difference in the values of w_e for the in-plane printed SCF/PA6 thin films without and with further CM processing. However, the interpretation of the relevant values of w_e is not straightforward, since the further CM processing also changed the orientation of the SCFs in the PA6 matrix, as shown earlier in Figure 6. Nevertheless, the quality of the in-plane printed SCF/PA6 composite thin film with the use of further CM processing is clearly significantly enhanced, compared to similar composite films with no further CM processing, since the value of R^2 is increased from 0.77 to 0.92. To improve the fusion bonding between filaments, it is worth mentioning that adopting CM during the 3D printing manufacturing process is not readily feasible. Instead, modification of the feedstock material, such as using a surface treatment for the reinforcement or some other in-process methods (e.g. adding an external heat source for controlling the temperature field, using some form of ultrasonic excitation, etc.) may be promising solutions and worthy of further exploration.

Thirdly, the discussions above have been based upon the trends, within a given feedstock material, shown in the values of w_e for the 3D printed films made using the SCF/PA6 composite filaments and the non-reinforced PA6 polymer filaments, via the FFF process. However, it is not possible to readily compare the absolute values of w_e for these two different filament materials in terms of identifying the extent of fusion bonding in these thin films. This is because the absolute value of w_e is a function not only of the extent of fusion bonding, i.e. the autohesion, between the filaments but also the inherent ductility of the film itself; and these two factors are not simply additive [30, 32, 33]. The non-reinforced PA6 polymer thin films, as discussed in detail in [18], are clearly far more ductile than the current SCF/PA6 composite thin films, and this prevents a direct comparison of the absolute values of w_e between the two types of thin films for the results shown in Table 1.

Finally, it should also be noted that both the weight fraction and length of the fibres were fixed in the current study, due to using only one type of feedstock filament. Therefore, a follow-up investigation may be beneficial to understand fully the effects of these two factors on the extent and quality of the fusion bonding between the SCF/PA6 filaments by the FFF process, using the proposed EWF method.

6. Conclusions

The present study has examined the extent and quality of the fusion bonding between individual filaments of short carbon-fibre reinforced polyamide 6 (SCF/PA6) composite that were deposited to manufacture thin films via 3D printing, employing the fused filament fabrication (FFF) process. Now, for good fusion bonding between the deposited filaments, a first key requirement is the attainment of intimate molecular contact between two filaments, so that the second key requirement of good intrinsic adhesion via molecular inter-diffusion (i.e. autohesion) between the two filaments can then occur.

The SCF/PA6 feedstock composite had 15 wt% of fibres present, with the lengths of the short fibres ranging from 35 µm to 245 µm, with an average of 105 µm. Significantly, these values are less than the nozzle diameter, i.e. 400 µm, of the equipment used for the FFF process. The SCF/PA6 composite thin films were deposited by an in-plane mode or an interlayer deposition mode, and also by the in-plane deposition mode followed by further compression moulding (CM). The SCFs were found to be preferentially aligned in the composite filaments along the printing path during the FFF process, with more than 83% and 99.8% of the SCFs oriented in an angle of ± 20° with respect to the printing direction for the in-plane (the *x*-*y* plane) and the interlayer (the *z*-*x* plane) deposition modes, respectively. However, further processing of the in-plane printed SCF/PA6 composite thin films using CM led to the SCFs becoming relatively random in their orientation.

The main characterisation technique employed was the essential work of fracture (EWF) method which has shown to be a valid approach and allows the evaluation of the extent and quality of the fusion bonding between the composite filaments by determining the value of the specific essential work of fracture, w_e, and the associated experimental reproducibility R^2, respectively. Further, to identify the process–structure–property relationships, the mesostructures of the films have also been identified.

The following conclusions can be drawn:

a) Undertaking EWF tests on 3D printed SCF/PA6 composite thin films has proven to be a feasible and efficient way to evaluate the extent and quality of fusion bonding between individual filaments of the 3D printed composite films. Such tests can provide a valuable insight into the printing quality of the FFF process.

b) For the 3D printed SCF/PA6 composite thin films, it was readily evident that the extent and quality of the fusion bonding, i.e. the adhesion via molecular inter-diffusion, often termed the autohesion, between the composite filaments was the weakest, and the most variable, in the composite thin films deposited via the interlayer mode. This was shown by such composite films possessing the lowest measured values of the specific essential work of fracture, w_e, and of the coefficient of determination, R^2, of 19.6 ± 3.9 kJ/m^2 and 0.05, respectively, of all the different types of 3D printed composite thin films that were studied.

c) The above observations in b) for the interlayer printed SCF/PA6 composite thin films arose from incomplete intimate contact between the composite filaments in these thin films, due to significant defects in the mesostructures being formed during the FFF process when the interlayer deposition mode was employed.

d) For the 3D printed SCF/PA6 composite thin films deposited via the in-plane mode, the use of a further compression moulding (CM) process appears to have had no significant effect on the extent of fusion bonding, since there was no significant difference in the values of w_e for the in-plane printed SCF/PA6 films without and with further CM processing. However, this conclusion is not straightforward since the further CM processing also changed the orientation of the SCFs in the PA6 matrix, leading to them becoming relatively random in orientation as opposed to being highly oriented in the direction of the composite filament for the in-plane printed SCF/PA6 thin films with no further CM processing. Nevertheless, the quality of the in-plane printed SCF/PA6 thin film was clearly significantly enhanced by the use of further CM processing, compared to those composite films with no further CM processing, since the value of R^2 increased from 0.77 to 0.92.

Acknowledgements

This work is supported by the Australian Research Council (Discovery Project #DP190102354). Access to the preparation, testing and characterisation facilities at the Centre for Advanced Materials Technology and the University of Sydney Microscopy & Microanalysis Centre is greatly appreciated.

References

[1] N. Turner B, Strong R, A. Gold S. A review of melt extrusion additive manufacturing processes: I. Process design and modeling. Rapid Prototyping Journal. 2014;20(3):192-204.
[2] Yang C, Tian X, Li D, Cao Y, Zhao F, Shi C. Influence of thermal processing conditions in 3D printing on the crystallinity and mechanical properties of PEEK material. Journal of Materials Processing Technology. 2017;248:1-7.
[3] Brenken B, Barocio E, Favaloro A, Kunc V, Pipes RB. Fused filament fabrication of fiber-reinforced polymers: A review. Additive Manufacturing. 2018;21:1-16.
[4] Stepashkin AA, Chukov DI, Senatov FS, Salimon AI, Korsunsky AM, Kaloshkin SD. 3D-printed PEEK-carbon fiber (CF) composites: Structure and thermal properties. Composites Science and Technology. 2018;164:319-26.
[5] Klift FVD, Koga Y, Todoroki A, Ueda M, Hirano Y, Matsuzaki R. 3D Printing of Continuous Carbon Fibre Reinforced Thermo-Plastic (CFRTP) Tensile Test Specimens. Open Journal of Composite Materials. 2016;Vol.06No.01:10.
[6] Kuznetsov VE, Solonin AN, Urzhumtsev OD, Schilling R, Tavitov AG. Strength of PLA Components Fabricated with Fused Deposition Technology Using a Desktop 3D Printer as a Function of Geometrical Parameters of the Process. Polymers. 2018;10(3):313.
[7] Domingo-Espin M, Puigoriol-Forcada JM, Garcia-Granada A-A, Llumà J, Borros S, Reyes G. Mechanical property characterization and simulation of fused deposition modeling Polycarbonate parts. Materials & Design. 2015;83:670-7.
[8] Ahn SH, Montero M, Odell D, Roundy S, Wright PK. Anisotropic material properties of fused deposition modeling ABS. Rapid Prototyping Journal. 2002;8(4):248-57.
[9] Shofner ML, Lozano K, Rodríguez-Macías FJ, Barrera EV. Nanofiber-reinforced polymers prepared by fused deposition modeling. Journal of Applied Polymer Science. 2003;89(11):3081-90.
[10] Ning F, Cong W, Qiu J, Wei J, Wang S. Additive manufacturing of carbon fiber reinforced thermoplastic composites using fused deposition modeling. Composites Part B: Engineering. 2015;80:369-78.
[11] Gray RW, Baird DG, Helge Bøhn J. Effects of processing conditions on short TLCP fiber reinforced FDM parts. Rapid Prototyping Journal. 1998;4(1):14-25.
[12] Quan Z, Larimore Z, Wu A, Yu J, Qin X, Mirotznik M, et al. Microstructural design and additive manufacturing and characterization of 3D orthogonal short carbon fiber/acrylonitrile-butadiene-styrene preform and composite. Composites Science and Technology. 2016;126:139-48.
[13] Goh GD, Dikshit V, Nagalingam AP, Goh GL, Agarwala S, Sing SL, et al. Characterization of mechanical properties and fracture mode of additively manufactured carbon fiber and glass fiber reinforced thermoplastics. Materials & Design. 2018;137:79-89.
[14] He Q, Wang H, Fu K, Ye L. 3D printed continuous CF/PA6 composites: Effect of microscopic voids on mechanical performance. Composites Science and Technology. 2020;191:108077.
[15] Tekinalp HL, Kunc V, Velez-Garcia GM, Duty CE, Love LJ, Naskar AK, et al. Highly oriented carbon fiber–polymer composites via additive manufacturing. Composites Science and Technology. 2014;105:144-50.
[16] Young D, Wetmore N, Czabaj M. Interlayer fracture toughness of additively manufactured unreinforced and carbon-fiber-reinforced acrylonitrile butadiene styrene. Additive Manufacturing. 2018;22:508-15.
[17] Papon EA, Haque A. Fracture toughness of additively manufactured carbon fiber reinforced composites. Additive Manufacturing. 2019;26:41-52.
[18] He Q, Ye L, Kinloch AJ, Wang H, Yin B. Characterisation of fusion bonding between filaments of thin 3D printed polyamide 6 using an essential work of fracture method. Journal of Materials Science. 2021;56(3):2777-94.
[19] Sun Q, Rizvi GM, Bellehumeur CT, Gu P. Effect of processing conditions on the bonding quality of FDM polymer filaments. Rapid Prototyping Journal. 2008;14(2):72-80.
[20] Abbott AC, Tandon GP, Bradford RL, Koerner H, Baur JW. Process-structure-property effects on ABS bond strength in fused filament fabrication. Additive Manufacturing. 2018;19:29-38.
[21] Bárány T, Czigány T, Karger-Kocsis J. Application of the essential work of fracture (EWF) concept for polymers, related blends and composites: A review. Progress in Polymer Science. 2010;35(10):1257-87.
[22] Ching ECY, Li RKY, Tjong SC, Mai Y-W. Essential work of fracture (EWF) analysis for short glass fiber reinforced and rubber toughened nylon-6. Polymer Engineering & Science. 2003;43(3):558-69.
[23] Tjong SC, Xu S-A, Li RK-Y, Mai Y-W. Mechanical behavior and fracture toughness evaluation of maleic anhydride compatibilized short glass fiber/SEBS/polypropylene hybrid composites. Composites Science and Technology. 2002;62(6):831-40.
[24] Chan WYF, Williams JG. Determination of the fracture toughness of polymeric films by the essential work method. Polymer. 1994;35(8):1666-72.
[25] Peng Y, Wu Y, Wang K, Gao G, Ahzi S. Synergistic reinforcement of polyamide-based composites by combination of short and continuous carbon fibers via fused filament fabrication. Composite Structures. 2019;207:232-9.
[26] Khanna YP, Kuhn WP. Measurement of crystalline index in nylons by DSC: Complexities and recommendations. Journal of Polymer Science Part B: Polymer Physics. 1997;35(14):2219-31.
[27] Fu S-y, Lauke B, Mai Y-w. Chapter 3 - Major factors affecting the performance of short fibre-reinforced polymers. In: Fu S-y, Lauke B, Mai Y-w, editors. Science and Engineering of Short Fibre-Reinforced Polymer Composites (Second Edition): Woodhead Publishing; 2019. p. 33-66.
[28] Prashantha K, Schmitt H, Lacrampe MF, Krawczak P. Mechanical behaviour and essential work of fracture of halloysite nanotubes filled polyamide 6 nanocomposites. Composites Science and Technology. 2011;71(16):1859-66.
[29] Tjong SC, Xu S-A, Li RKY, Mai YW. Fracture characteristics of short glass fibre/maleated styrene–ethylene–butylene–

styrene/polypropylene hybrid composite. Polymer International. 2002;51(11):1248-55.
[30] Kinloch AJ. Adhesion and adhesives: Science and technology: Springer, Dordrecht; 1987.
[31] Bhandari S, Lopez-Anido RA, Gardner DJ. Enhancing the interlayer tensile strength of 3D printed short carbon fiber reinforced PETG and PLA composites via annealing. Additive Manufacturing. 2019;30:100922.
[32] Andrews EH, Kinloch AJ, Melville HW. Mechanics of adhesive failure. I. Proceedings of the Royal Society of London A Mathematical and Physical Sciences. 1973;332(1590):385-99.
[33] Andrews EH, Kinloch AJ, Melville HW. Mechanics of adhesive failure. II. Proceedings of the Royal Society of London A Mathematical and Physical Sciences. 1973;332(1590):401-14.

Figures and Tables Captions:

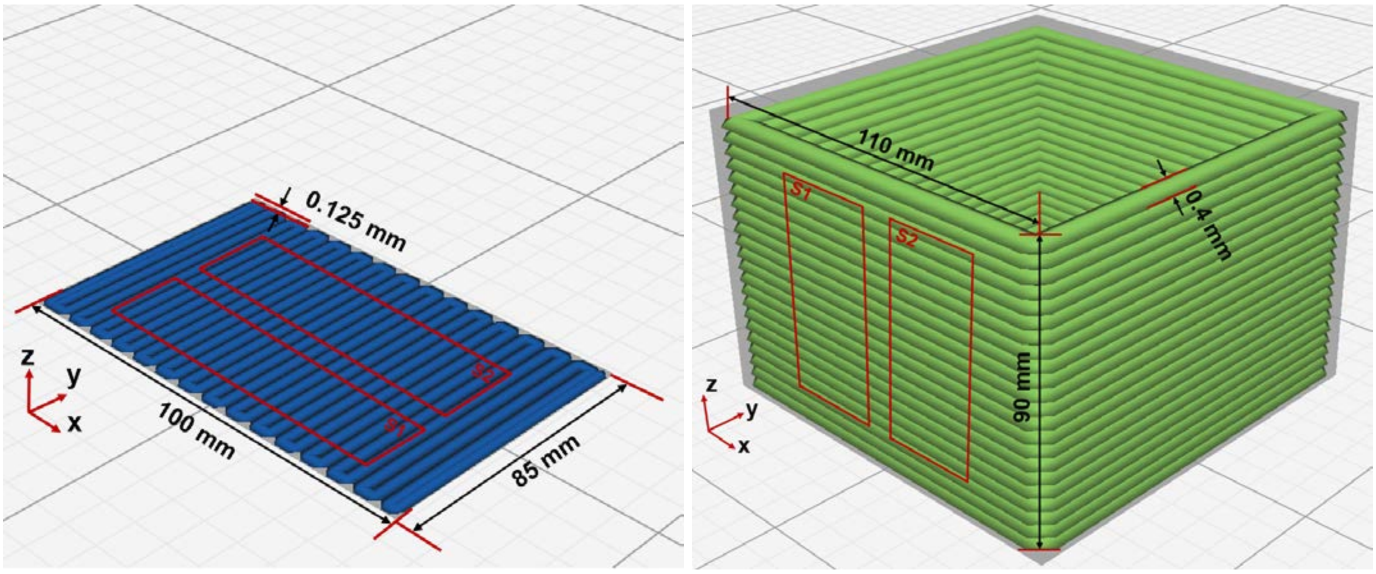

(a) (b)

Figure 1. Schematic of the printed double edge-notched tension (DENT) specimens with the deposition path of the SCF/PA6 filaments shown: (a) a single-layer film 3D printed in the *x*-*y* plane via the in-plane deposition mode and (b) a single-filament box 3D printed via the interlayer deposition mode. The fused filament fabrication (FFF) process was used to manufacture all the specimens. The orientations of the DENT specimens, labelled ‘S1’ and ‘S2’, are also indicated.

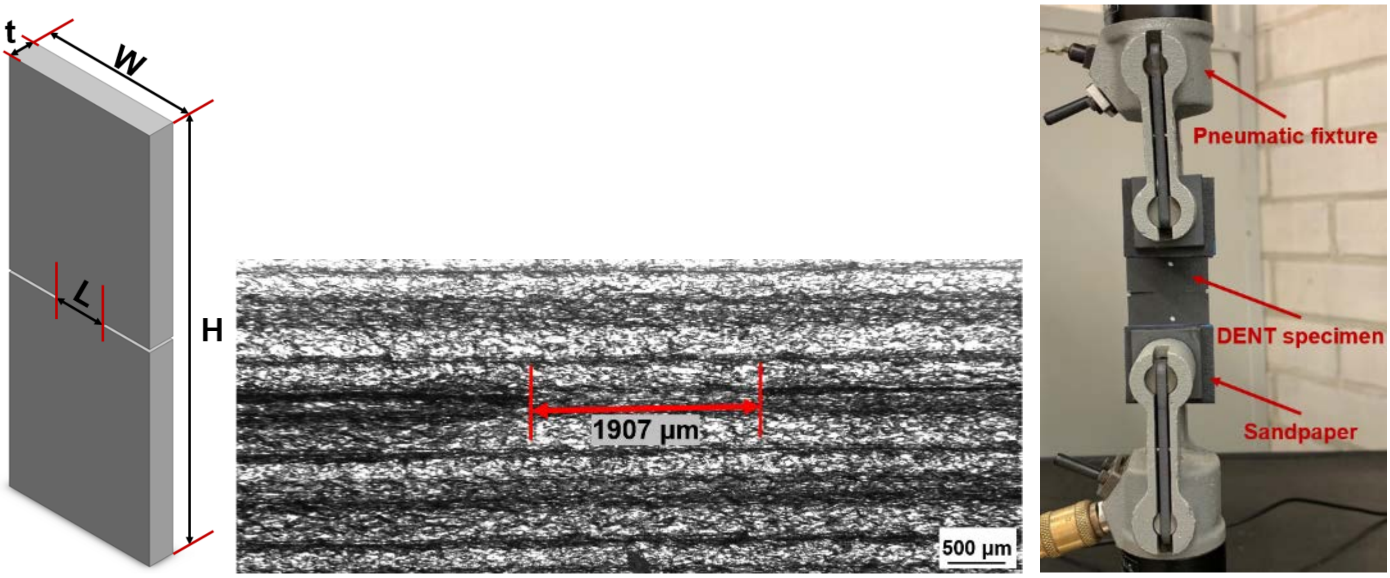

(a) (b) (c)

Figure 2. The double edge-tension (DENT) specimen and test: (a) schematic, (b) an optical micrograph of a nominally 2 mm long ligament in a SCF/PA6 composite thin film and (c) an essential work of fracture (EWF) test.

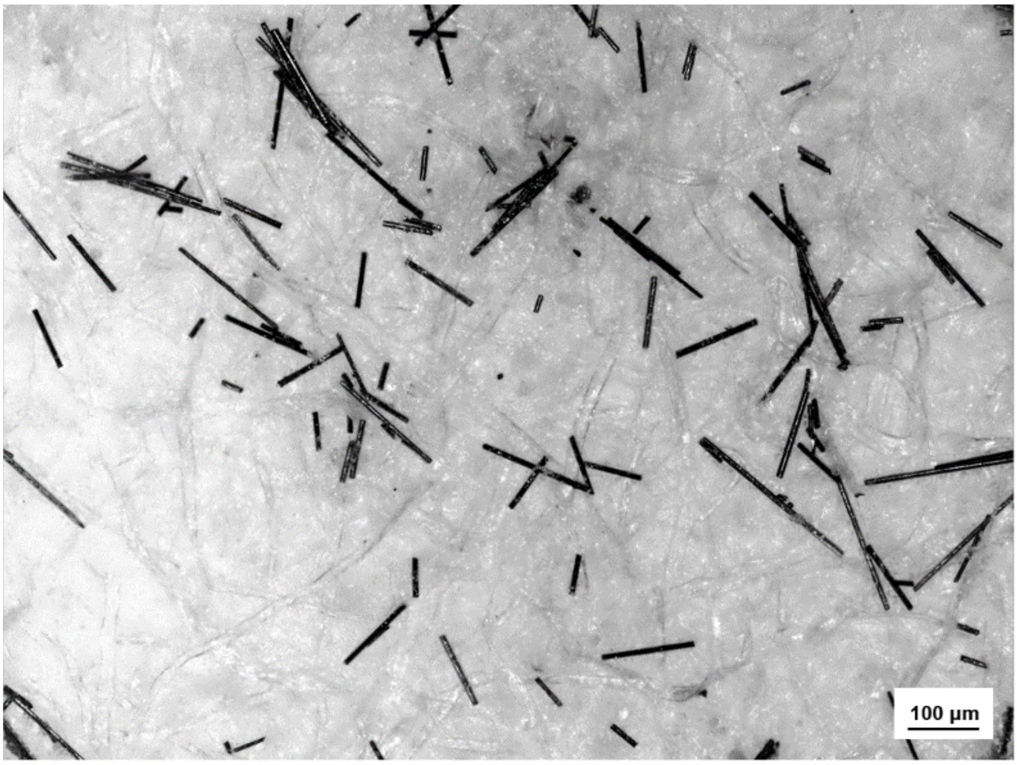

Figure 3. Optical micrograph of the SCFs from the SCF/PA6 composite feedstock filament, after removing the PA6 matrix.

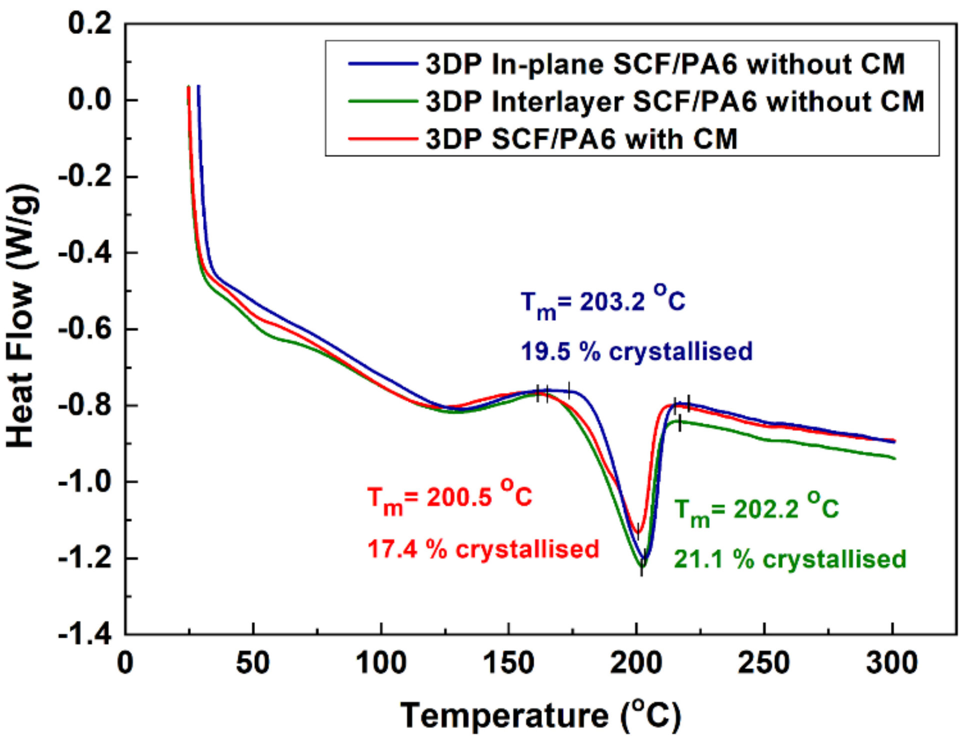

Figure 4. Typical DSC curves of the 3D printed SCF/PA6 composite thin films.

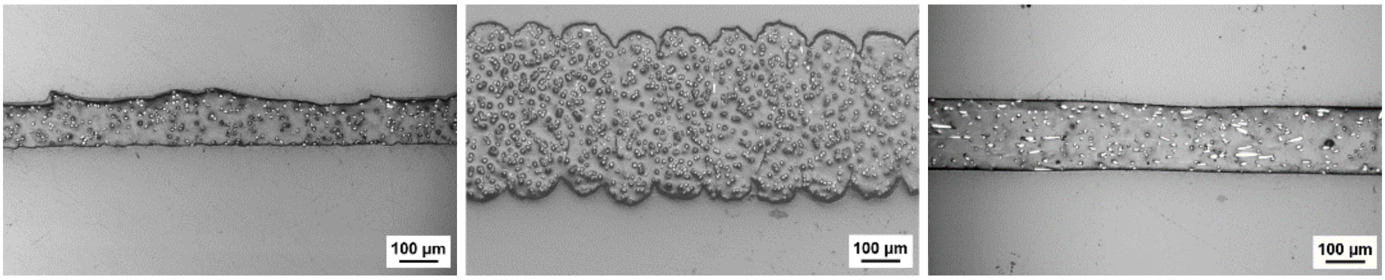

(a) (b) (c)

Figure 5. Optical micrographs of typical cross-sections of the FFF manufactured composite thin films: (a) the in-plane printed SCF/PA6, (b) the interlayer printed SCF/PA6, and (c) the in-plane printed SCF/PA6 with further CM processing.

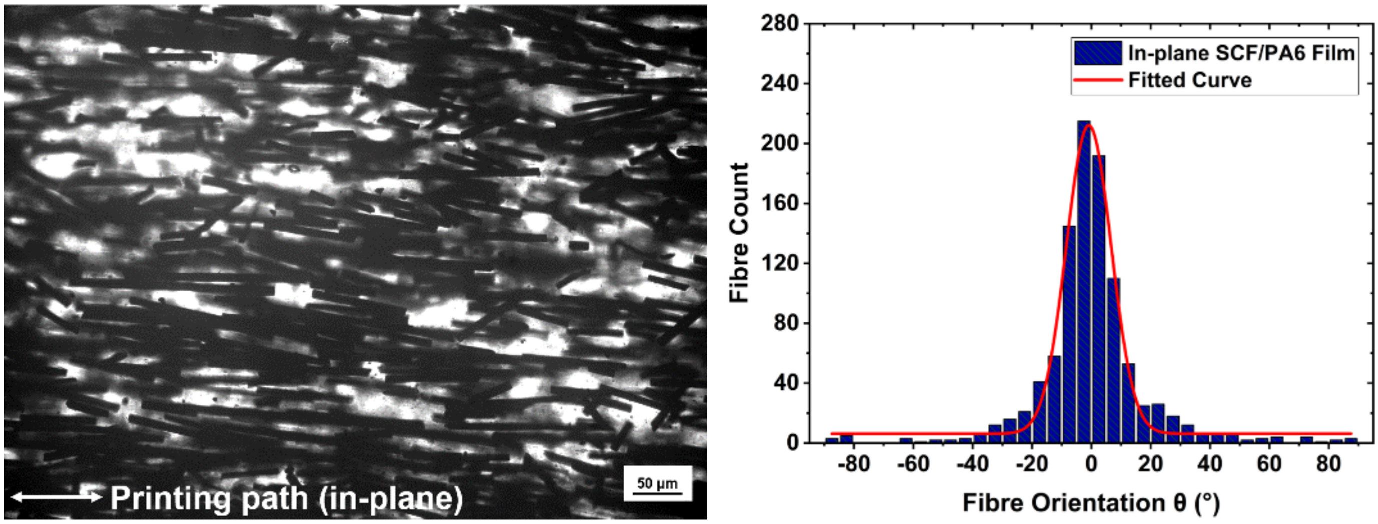

(a)

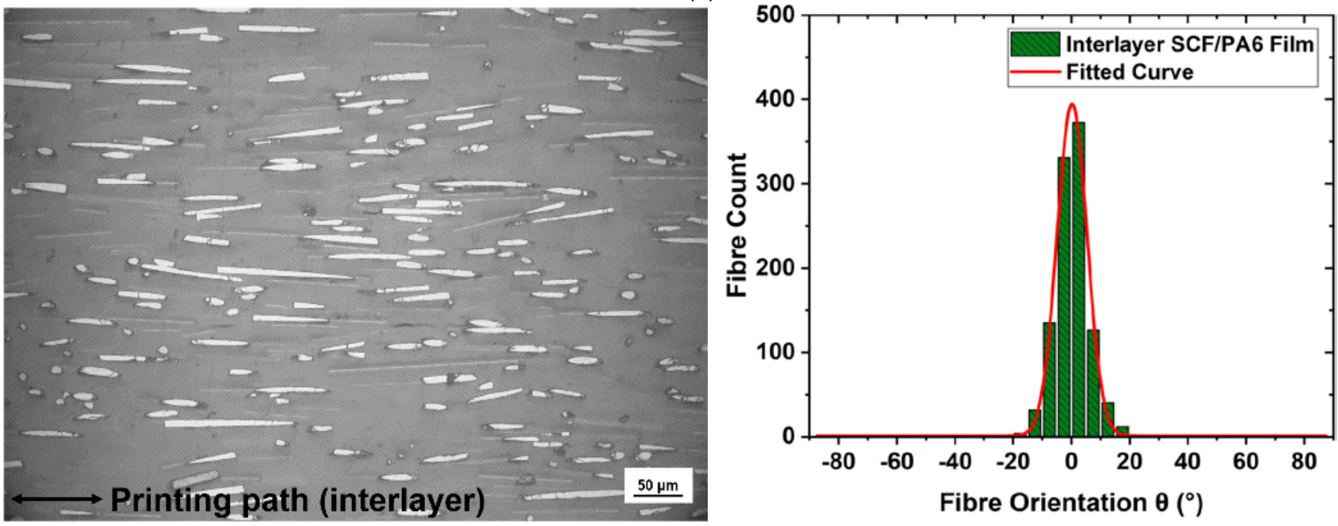

(b)

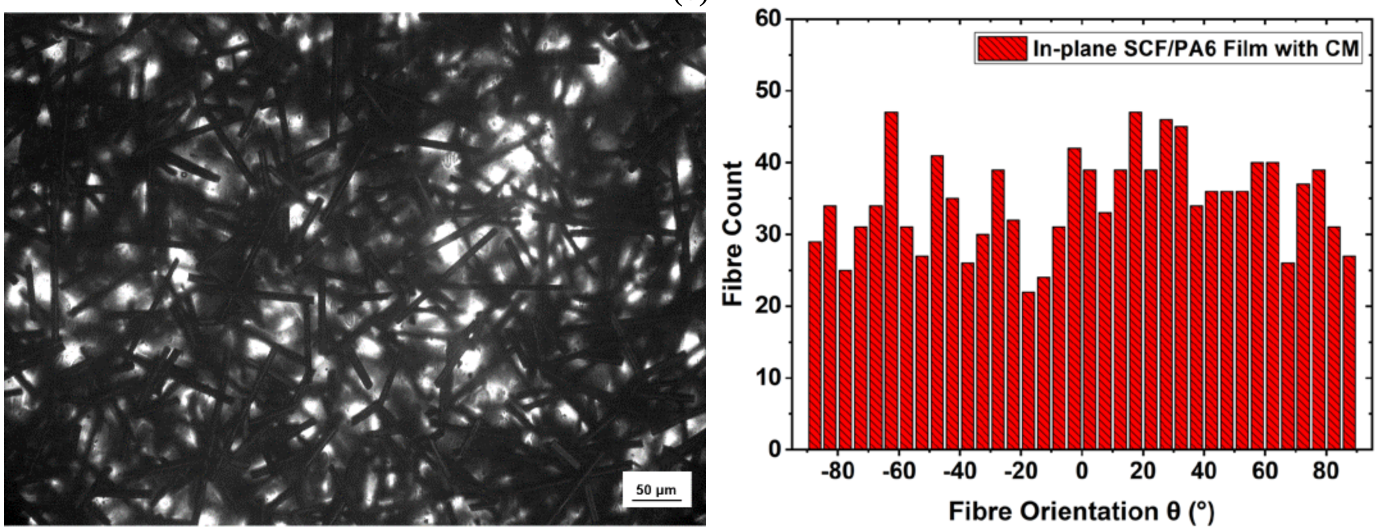

(c)

Figure 6. Micrographs and statistical data showing the fibre orientation within the composite thin films: (a) the in-plane printed SCF/PA6, (b) the interlayer printed SCF/PA6 and (c) the in-plane printed SCF/PA6 with further CM processing.

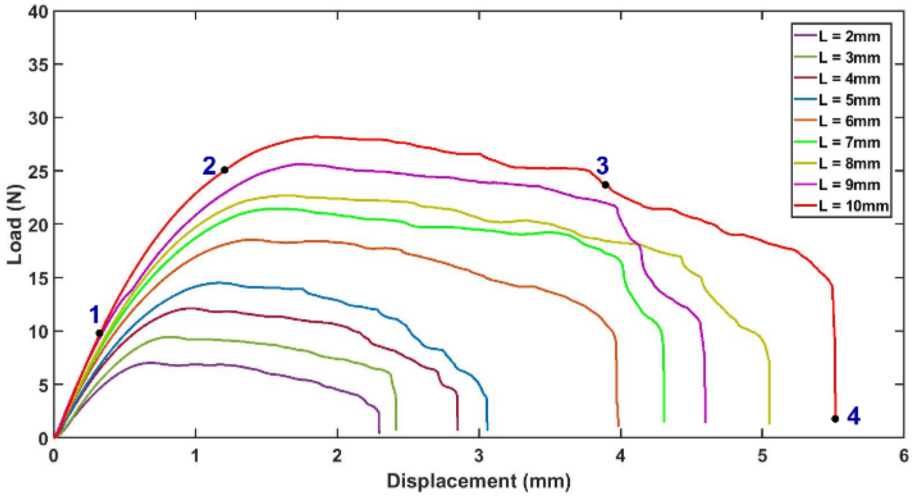

(a)

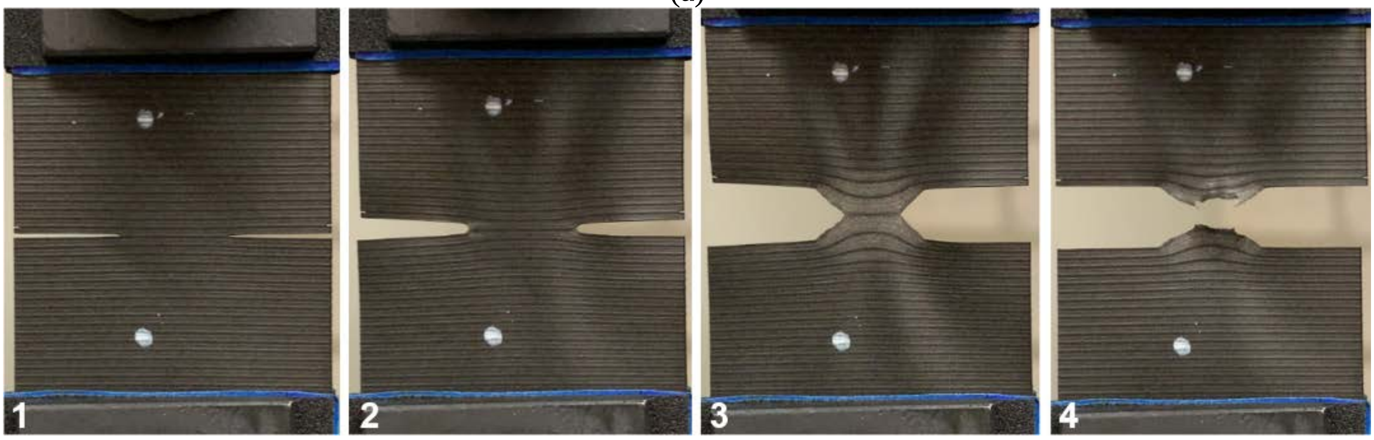

(b)

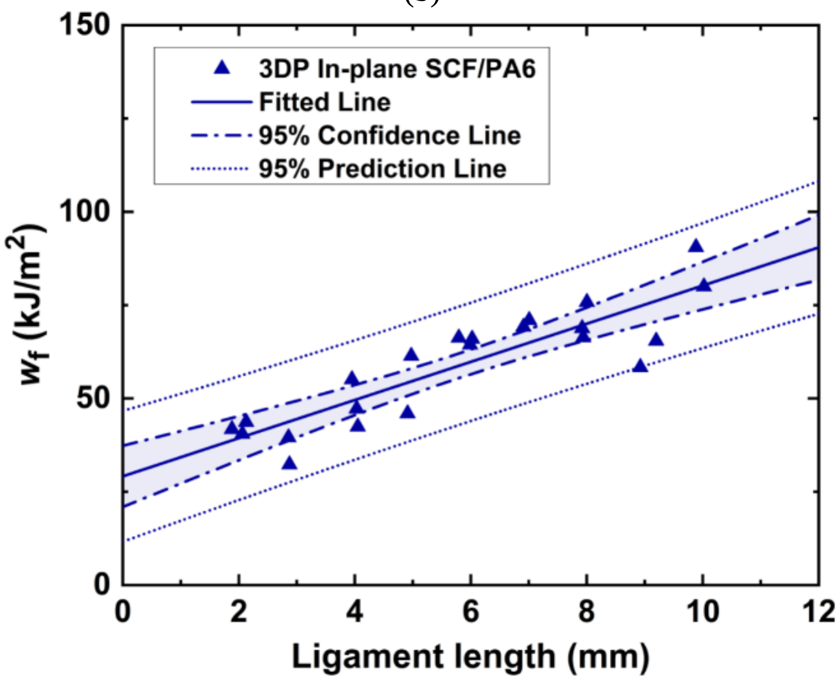

(c)

Figure 7. Results from the EWF tests on the in-plane printed SCF/PA6 composite thin films: (a) typical load versus displacement curves, (b) the fracture behaviour recorded during the test for a DENT specimen with a nominal 10 mm ligament length (the numbers refer to corresponding positions on the load versus displacement curve for this specimen as shown in Figure 7 (a)) and (c) a plot of the total specific work of fracture, w_f, versus the ligament length, L, with the 95% confidence and prediction lines shown.

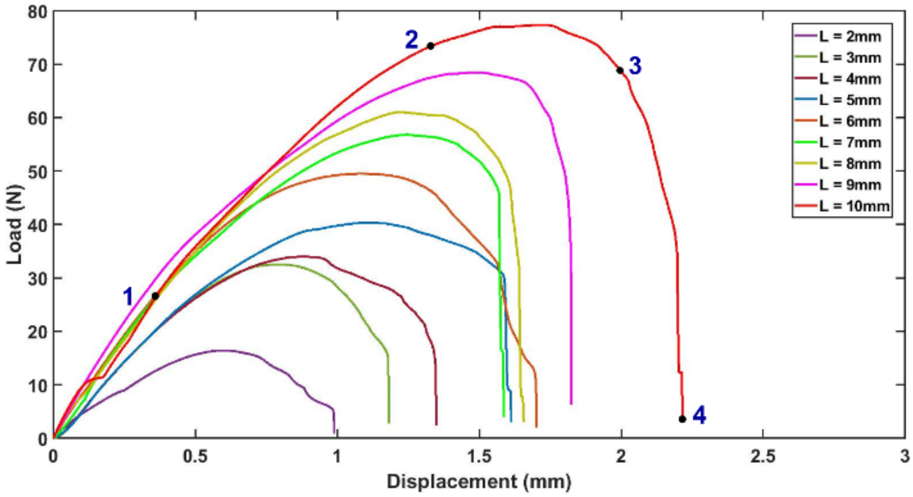

(a)

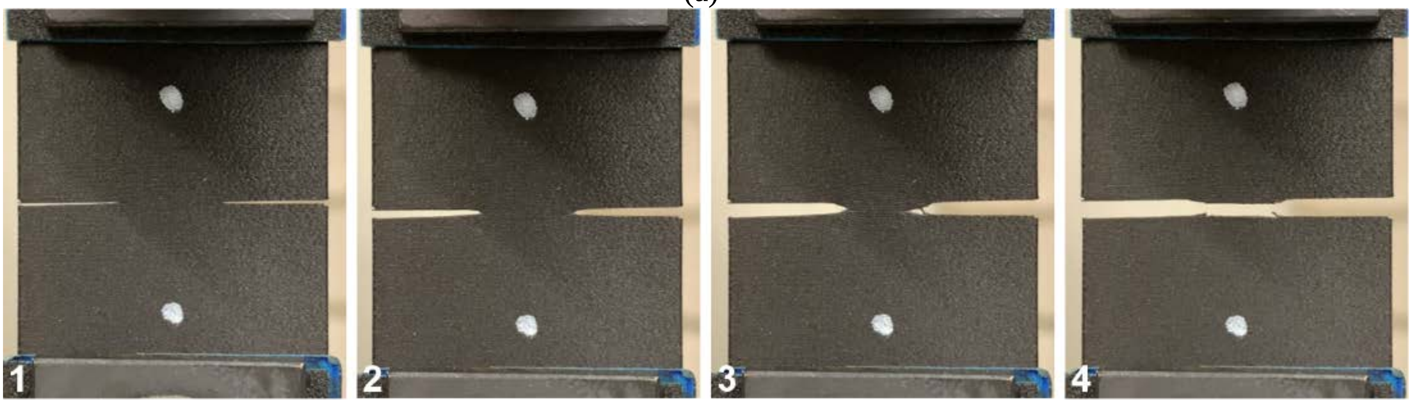

(b)

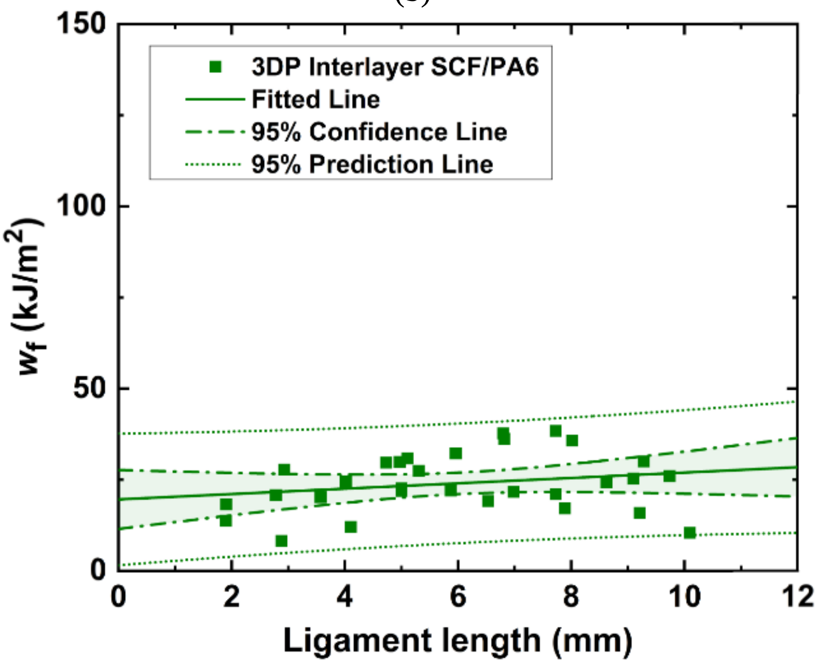

(c)

Figure 8. Results from the EWF tests on the interlayer printed SCF/PA6 composite thin films: (a) typical load versus displacement curves, (b) the fracture behaviour recorded during the test for a DENT specimen with a nominal 10 mm ligament length (the numbers refer to the corresponding positions on the load versus displacement curve for this specimen as shown in Figure 8 (a)) and (c) plot of the total specific work of fracture, w_f, versus the ligament length, L, with the 95% confidence and prediction lines shown.

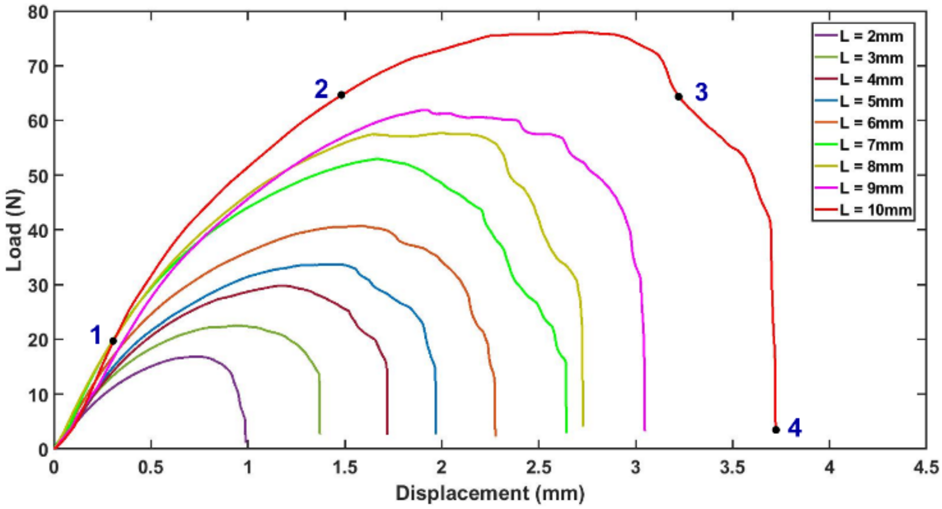

(a)

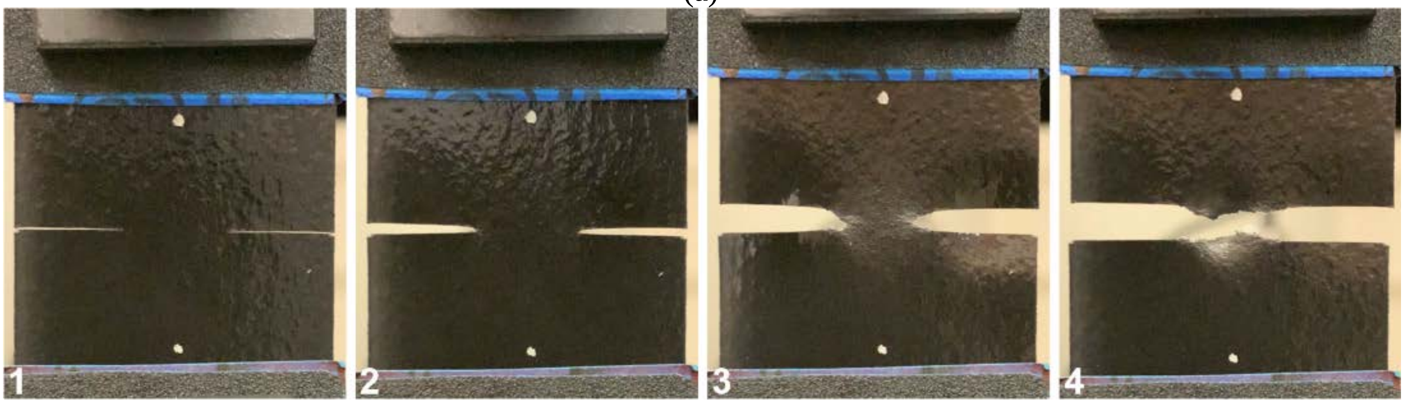

(b)

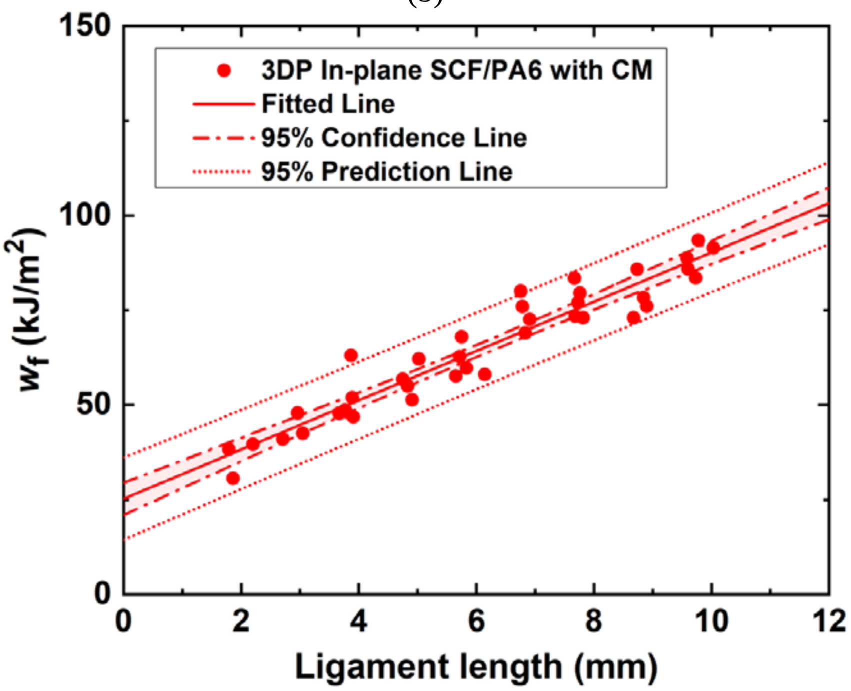

(c)

Figure 9. Results from the EWF tests on the in-plane printed SCF/PA6 composite thin films with further compression moulding (CM): (a) typical load versus displacement curves, (b) the fracture behaviour recorded during the test for a DENT specimen with a nominal 10 mm ligament length (the numbers refer to the corresponding positions on the load versus displacement curve for this specimen as shown in Figure 9 (a)) and (c) a plot of the total specific work of fracture, w_f, versus the ligament length, L, with the 95% confidence and prediction lines shown.

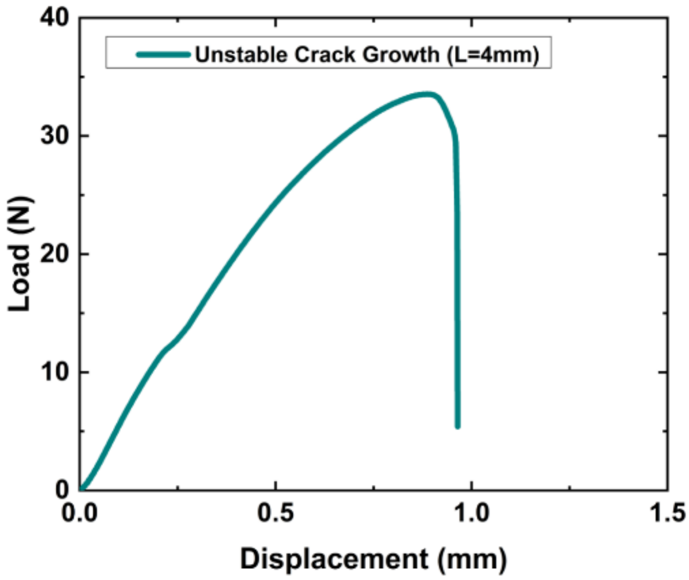

(a)

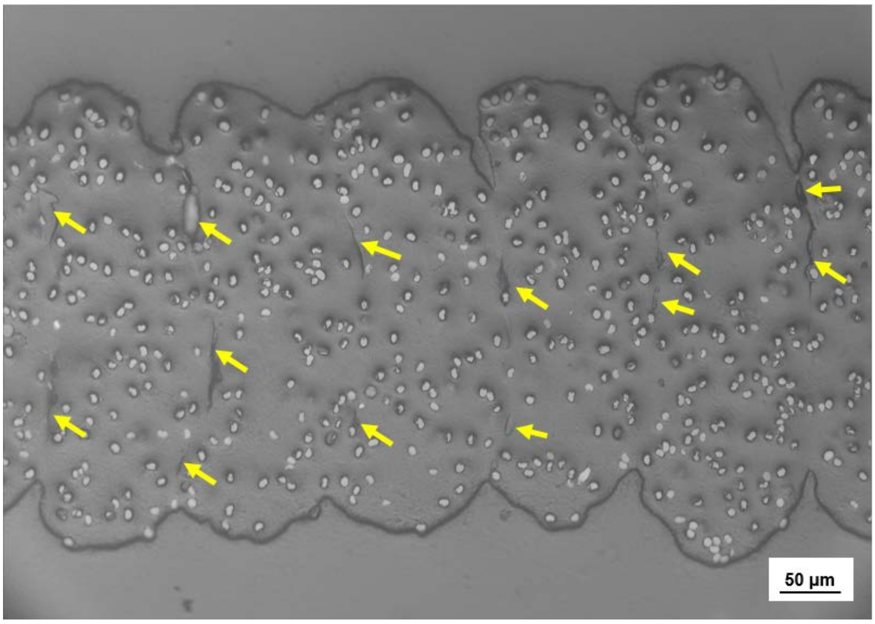

(b)

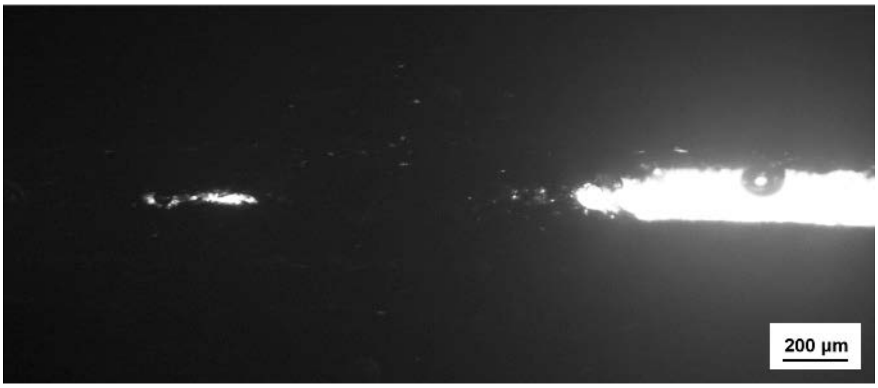

(c)

Figure 10. Fracture behaviour and mesostructures of the interlayer printed SCF/PA6 composite thin films when unstable crack growth occurs: (a) load versus displacement curve from a DENT specimen for unstable crack growth during the EWF test, (b) optical micrograph showing incomplete fusion between filaments and the defects, e.g. voided areas, are indicated by the yellow arrows, and (c) voids developing ahead of a main crack tip during the EWT test.

Table 1. EWF test results for the 3D printed SCF/PA6 composite thin films (present work) and for the non-reinforced (i.e. pure) PA6 polymer thin films [18].

	SCF/PA6 (in-plane)	PA6 [18] (in-plane)	SCF/PA6 (interlayer)	PA6 [18] (interlayer)	SCF/PA6 (in-plane with CM)	PA6 [18] (in-plane with CM)
w_e (kJ/m^2)	29.2 ± 3.9	25.7 ± 3.1	19.6 ± 3.9	21.3 ± 9.1	25.2 ± 2.1	38.1 ± 3.1
R^2	0.77	0.92	0.05	0.50	0.92	0.96